Graphical interpretation deformation analysis of stability area using of strain analysis

Slavomír Labant [1], **Gabriel Weiss**[1], **Jozef Zuzik**[2] and **Michal Baran**[1]

The spatial changes of water construction objects are surveyed by geodetic methods within the technical and safety supervision of water constructions. To better understand the behaviour of the area of interest beneath the upper reservoir of the pumped storage hydro power plant (PSHPP) Čierny Váh, a deformation analysis of this area was realized. The stability or instability of the geodetic network points and the adjacent area was verified. The estimations of determined parameters of geodetic network were obtained on the basis of stage adjustment of GNSS observations, by applying the LSM method, robust M-estimation according to Huber and robust M-estimation according to Hampel. The analysis of incurred discrepancies (differences) in the position of points, whether they are the results of accumulation of measurement and systematic errors or they represent a local deformation of the area, was the last objective of this papier. The analysis of the results obtained from processing was performed by the method of finite elements in the form of strain analysis, to present the dynamics of the area underneath the water reservoir. The results obtained by applying estimation methods correspond to their graphical analysis. The use of Huber's and Hampel's robust M-estimates is an alternative to the application of LSM method, which has a versatile use in practice, in various areas of professional disciplines.

Key words: *Deformation analysis, LSM, Huber's robust M-estimate, Hampel's robust M-estimate, Strain analysis*

Introduction

The Earth surfaces, but also objects on and underneath it, are affected by external as well as internal forces that deform these objects. Nowadays, modern Global Navigation Satellite Systems (GNSS) are increasingly being used for deformation monitoring of the Earth's surface and objects on it. The advantages of GNSS observations, mainly a great reliability, independence of the season, time of measurement or direct visibility between points are widely used, while the term observation in real time is getting more and more into the foreground. In the real-time monitoring, the measurements in epochs dominate in regard of the price and protection of instrumentation.

The stability monitoring of dynamically loaded water constructions is elaborated in the "Technical and Safety Supervision" approved by the Ministry of Environment of the Slovak Republic. Details about the safety of water constructions are specified in the Act No. 364/2004 Coll. on waters, amending Act No. 372/1990 Coll. of the Slovak National Council on offences, as amended by later regulations (Water Act) [23].

Adjustment methods

Methods of adjustment are based on the minimum condition of some norm of the vector of corrections. The norm is a number assigned to each n-dimensional vector that characterizes its size. Objective functions of following types are the most commonly used in geodesy [1], [2]:

$$\rho(v_i) = \left(\sum_{i=1}^{n} |v_i|^p \right)^{\frac{1}{p}} = \min . \qquad (1)$$

The p parameter specifies a special type of an objective function [3]:

The method of the minimum sum of absolute values of corrections *with the parameter* p=1 (L1-norm) *is expressed by the objective function:*

$$\rho(v_i) = \sum_{i=1}^{n} |v_i| = \min . \qquad (2)$$

[1] *Assoc. prof. MSc. Slavomír Labant, PhD., prof. MSc. Gabriel Weiss, PhD., MSc. Michal Baran, PhD.,* Institute of Geodesy, Cartography and GIS, F BERG, Technical University of Košice, Letná 9, 042 00 Košice, Slovak Republic, slavomir.labant@tuke.sk, gabriel.weiss@tuke.sk, michal.baran@tuke.sk

[2] *MSc. Jozef Zuzik, PhD.,* Institute of Business and Management, F BERG, Technical University of Košice, Letná 9, 042 00 Košice, Slovak Republic, jozef.zuzik@tuke.sk

Least Squares Method (LSM) with the parameter *p=2 (L2-norm)* is expressed by the objective function:

$$\rho(v_i) = \left(\sum_{i=1}^{n} v_i^{\,2} \right)^{\frac{1}{2}} = \min . \tag{3}$$

The MINIMAX method with the parameter for $p = \infty$ (L^{∞} - norm – measurements are defined by tolerance intervals) is expressed by the objective function:

$$\rho(v_i) = \left(\sum_{i=1}^{n} |v_i|^{\infty} \right)^{\frac{1}{\infty}} = \min . \tag{4}$$

Identifying and locating of mistakes and systematic errors weighting some of measured variables that would be either cleaned or excluded from files entering the adjustment procedure is the objective of reliable processing of measured variables prior to their evaluation. The LSM provides an unbiased and the best estimate only for normal distribution of errors in the set of measured variables. If the measured variables are weighted by systematic errors and mistakes (yawing values), the LSM is still effectively usable. This method also has the feature that larger errors of variables tries to decompose into smaller parts, thereby unacceptably distorting estimates of adjustment procedure [15], [16], [19], [21].

Defects with the LSM led statistics to seek methods which are more resistant (robust) using remote measurement. Experiments have shown that robust estimates give better results than the LSM. The majority of robust adjustments used in geodesy modify the existing LSM to make it robust. When using the robust LSM, the weight of measurement changes in each iteration using the weight function.

When using the robust method for estimation, the minimised function $v^T v$ is replaced with the so-called loss function [5], [9]: $\rho(v_i) = \min$, which generates the influence function $\psi(v_i)$ characterising the influence of errors upon adjusted values. For this function, the following is valid:

$$\sum_{i=1}^{n} \psi(v_i) = 0 \text{, where } \psi(v_i) = \frac{\partial \rho(v_i)}{\partial v_i}. \tag{5}$$

In order that the adjustment will have the nature of a robust estimate, it is suitable to carry it out using the iteration method with variable weighing, i.e. that the weight p_i of observation l_{ij} was determined in each iteration step as a corrective function:

$$p(v_i) = \frac{\psi(v_i)}{v_i}, \text{ where } p(v_i) \text{ is the weight function.} \tag{6}$$

This principle of solution is iterative solution with gradually changing weights measured variables p_i so that when a sufficient number of iteration cycles (steps) were convergence corrections in the last step. The most used estimates are Huber's robust M-estimate, Hampel's robust M-estimate, for more information and function of estimates see [14].

Observations and processing of geodetic network

Points of the geodetic network are located around the crest of upper reservoir of the hydro power plant Čierny Váh in the area of the National Park Low Tatras. PSHPP is used mainly for hydraulic energy storage in times of reduced electric system load, therefore preventing a wasteful shutting down of thermal (or nuclear) power plants or reducing their performance to the operational minimum. The issue of efficient use of hydropower is currently in the process of sustainable development of each country often addressing question [9]. In relation with the solution of the issue, it should also take into account the natural character of the flood risks that may endanger the subject area [10]. Geographic approach to flood risk assessment provides an appropriate tool to present the obtained results [5]. GNSS technology, in contrast to terrestrial technologies, is not dependent on the direct visibility between points. Therefore, it is not necessary to make forest paths through bushy or forest stand in areas of increased protection of nature. Seven reference points are monumented by heavy monumentation around the reservoir, labelled numerically in the range 5001 - 5007 (Fig. 1). The observations were realized in epochs April 2004, July 2008 and October 2011 for the purpose of deformation monitoring of stability or instability of observed points of the geodetic network. The network was realized by 11 GNSS vectors with the structure of geodetic network in the shape of heptagon in each epoch.

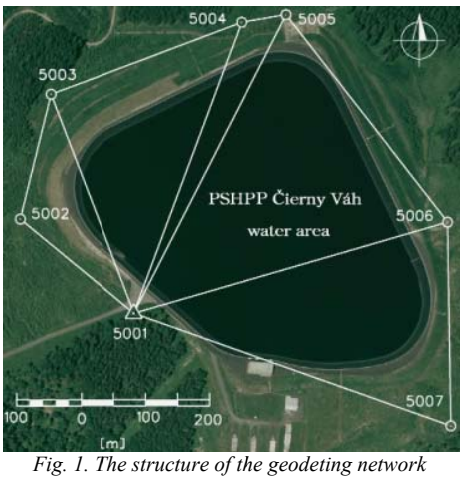

Fig. 1. The structure of the geodeting network

A Gauss Markov model (GMM) is the most commonly used method for adjustment of a general geodetic network, defined as follows [14], [17], [18], [20], [21]:

$$\begin{aligned} \mathbf{v} &= \mathbf{A}\mathbf{d}\hat{\mathbf{C}} - \mathbf{d}\mathbf{L} = \mathbf{A}(\hat{\mathbf{C}} - \mathbf{C}^{\circ}) - (\mathbf{L} - \mathbf{L}^{\circ}), && \text{- functional part,} \\ \boldsymbol{\Sigma}_{\mathbf{L}} &= s_0^2 \mathbf{Q}_{\mathbf{L}}, && \text{- stochastic part,} \end{aligned} \tag{7}$$

where: $\mathbf{v}$ is a vector of corrections of observed values, $\mathbf{dL=L-L^{\circ}}$ is a vector of auxiliary observations, $\mathbf{d}\hat{\mathbf{C}}=\hat{\mathbf{C}}-\mathbf{C}^{\circ}$ is a vector of complements of adjusted values of determining coordinates, $\mathbf{A}$ is a design matrix.

The adjustment procedure consists of the following steps:

1. arrangement of the input data,
2. definition of model equations,
3. auxiliary calculations,
4. creation of a configuration matrix,
5. calculation of estimations,
6. expression of the accuracy of a geodetic network.

Data of GPS and GNSS vectors that were measured and primary processed by software were subsequently processed based on the Gauss-Markov estimation model (GMM – adjustment of indirect measurements) as a GMM with full rank. The point 5001 was selected as the reference point of the geodetic network (monumented in the original and most plain terrain, GNSS receiver remained in the position during the whole measurement). Spatial orthogonal coordinates X_i, Y_i, Z_i and coordinate differences $\Delta X_{ij}, \Delta Y_{ij}, \Delta Z_{ij}$ between individual network points in ETRS89 were the result of processing.

The observation vector $\mathbf{L}$ consist of $3\,x\,11$ spatial vectors of observations ΔXYZ_{ij}, i.e. $3\,x\,33$ of observation components $\Delta X_{ij}, \Delta Y_{ij}, \Delta Z_{ij}$. The three-variant processing and adjustment of observations and determined estimations of adjusted coordinates was used for the processing of deformation network observed in three epochs for functional part of GMM $(\tau = 04,08,11)$:

$$\underset{(99,1)}{\begin{pmatrix} {}^{04}\mathbf{v} \\ {}^{08}\mathbf{v} \\ {}^{11}\mathbf{v} \end{pmatrix}} = \underset{(99,54)}{\begin{pmatrix} {}^{04}\mathbf{A} & & 0 \\ & {}^{08}\mathbf{A} & \\ 0 & & {}^{11}\mathbf{A} \end{pmatrix}} \cdot \underset{(54,1)}{\begin{pmatrix} {}^{04}\mathbf{d}\hat{\mathbf{C}} \\ {}^{08}\mathbf{d}\hat{\mathbf{C}} \\ {}^{11}\mathbf{d}\hat{\mathbf{C}} \end{pmatrix}} - \underset{(99,1)}{\begin{pmatrix} {}^{04}\mathbf{dL} \\ {}^{08}\mathbf{dL} \\ {}^{11}\mathbf{dL} \end{pmatrix}}, \tag{8}$$

Coordinate values of determined points of the network $\hat{\mathbf{C}}$ are dependent on the used estimation method of unknown parameters (LSM, robust M-estimation according to Huber, robust M-estimation according to Hampel). Estimates of adjusted coordinates $\hat{\mathbf{C}}$ are presented in Tab. 1.

Tab. 1. ETRS89 coordinates X, Y, Z from adjustment by the LSM method and robust M-estimation according to Huber and Hampel

	Point	LSM			Huber			Hampel		
		$\hat{X}_{ETRS89}$ [m]	$\hat{Y}_{ETRS89}$ [m]	$\hat{Z}_{ETRS89}$ [m]	$\hat{X}_{ETRS89}$ [m]	$\hat{Y}_{ETRS89}$ [m]	$\hat{Z}_{ETRS89}$ [m]	$\hat{X}_{ETRS89}$ [m]	$\hat{Y}_{ETRS89}$ [m]	$\hat{Z}_{ETRS89}$ [m]
	5002	3 941 063.358	1 427 021.983	4 792 984.567	3 941 063.358	1 427 021.984	4 792 984.567	3 941 063.358	1 427 021.984	4 792 984.567
	5003	0 896.381	6 998.783	3 089.955	0 896.381	6 998.783	3 089.955	0 896.382	6 998.783	3 089.955
	5004	0 722.170	7 243.221	3 194.259	0 722.170	7 243.220	3 194.259	0 722.171	7 243.220	3 194.259
	5005	0 690.589	7 304.206	3 208.553	0 690.590	7 304.206	3 208.552	0 690.590	7 304.206	3 208.552
	5006	0 816.179	7 638.525	3 016.659	0 816.180	7 638.524	3 016.659	0 816.180	7 638.524	3 016.659
	5007	1 027.267	7 741.653	2 811.096	1 027.267	7 741.652	2 811.096	1 027.267	7 741.652	2 811.096
	5002	3 941 063.360	1 427 021.986	4 792 984.571	3 941 063.360	1 427 021.985	4 792 984.571	3 941 063.360	1 427 021.985	4 792 984.571
	5003	0 896.375	6 998.784	3 089.950	0 896.375	6 998.783	3 089.951	0 896.375	6 998.783	3 089.950
	5004	0 722.168	7 243.221	3 194.260	0 722.167	7 243.223	3 194.260	0 722.167	7 243.223	3 194.260
	5005	0 690.584	7 304.226	3 208.559	0 690.584	7 304.226	3 208.560	0 690.584	7 304.227	3 208.560
	5006	0 816.169	7 638.519	3 016.661	0 816.169	7 638.517	3 016.663	0 816.169	7 638.518	3 016.662
	5007	1 027.259	7 741.649	2 811.098	1 027.259	7 741.648	2 811.099	1 027.259	7 741.649	2 811.099
	5002	3 941 063.364	1 427 021.989	4 792 984.566	3 941 063.364	1 427 021.990	4 792 984.566	3 941 063.364	1 427 021.990	4 792 984.566
	5003	0 896.378	6 998.786	3 089.953	0 896.378	6 998.788	3 089.953	0 896.377	6 998.788	3 089.953
	5004	0 722.170	7 243.214	3 194.264	0 722.170	7 243.214	3 194.265	0 722.170	7 243.214	3 194.265
	5005	0 690.579	7 304.220	3 208.561	0 690.578	7 304.220	3 208.563	0 690.578	7 304.220	3 208.563
	5006	0 816.174	7 638.516	3 016.657	0 816.174	7 638.516	3 016.659	0 816.174	7 638.516	3 016.660
	5007	1 027.261	7 741.644	2 811.092	1 027.261	7 741.644	2 811.093	1 027.261	7 741.644	2 811.094

Coordinate transformation from ETRS89 to UTCN03

A global transformation key is used for transformation of points coordinates from the ETRS89 system into the national implementation UTCN03 of the coordinate system UTCN, that applies to the whole territory of the SR and is defined by seven transformation parameters determined by spatial similarity transformation by the Burša-Wolf´s model [24].

Transformation parameters for transition from the GRS 80 to the Bessel ellipsoid 1841 are [24]:

- translations: $T_X = -485.021$ m, $T_Y = -169.465$ m, $T_Z = -483.839$ m,
- rotations: $R_X = 7.786342''$, $R_Y = 4.397554''$, $R_Z = 4.102655''$,
- scaling: m = 0.0 ppm.

Cartesian spatial coordinates of points related to the Bessel ellipsoid 1841 from the GRS 80 ellipsoid are obtained by spatial similarity transformation by the Burša-Wolf´s model (or Molodenskij-Badekas model).

The transformation of Cartesian coordinates *X,Y,Z* to ellipsoidal coordinates *φ, λ* and *h* is the next step. Conversion of coordinates *φ, λ* and *h* to orthogonal planar coordinates of conform conic projection in a general position is realized by Křovák´s universe projection.

A digital reference elevation model with the alphabetical DVRM code with the step of *600 x 600 m* is used for conversion of ellipsoidal heights determined in the ETRS89 and defined above the GRS80 ellipsoid to normal heights defined in The Baltic Vertical Datum after adjustment (Bpv). This digital model was created by fitting the gravimetric quasi-geoid GMSQ03B to points of The National Spatial Network with the known levelled height determined in The National Levelling Network [12].

As an alternative of long calculations of coordinate transformations from the ETRS89 to the national implementation UTCN03 [7], [8] a suitable software that allows such a transformation can be used, for example Leica Geo Office. In this way, also adjusted coordinates of points of all three epochs determined by the LSM and robust estimations according to Huber and Hampel were transformed (Tab. 2).

Tab. 2. UTCN03 coordinates X, Y, h from adjustment by the LSM method and according to Huber and Hampel.

$^{\tau}t$	Point	LSM			Huber			Hampel		
		X_{UTCN03} [m]	Y_{UTCN03} [m]	h_{Bpv} [m]	X_{UTCN03} [m]	Y_{UTCN03} [m]	h_{Bpv} [m]	X_{UTCN03} [m]	Y_{UTCN03} [m]	h_{Bpv} [m]
^{04}t	5002	1 200 717.584	360 041.445	1 151.443	1 200 717.584	360 041.444	1 151.443	1 200 717.584	360 041.444	1 151.443
	5003	0 526.676	59 994.052	22.868	0 526.676	59 994.052	22.868	0 526.677	59 994.052	22.868
	5004	0 416.325	59 697.273	48.783	0 416.325	59 697.274	48.783	0 416.325	59 697.274	48.783
	5005	0 404.623	59 628.302	53.728	0 404.624	59 628.303	53.722	0 404.624	59 628.303	53.722
	5006	0 722.297	59 376.688	60.944	0 722.298	59 376.689	60.944	0 722.298	59 376.689	60.944
	5007	1 034.337	59 371.644	58.938	1 034.337	59 371.645	58.938	1 034.337	59 371.645	58.938
^{08}t	5002	1 200 717.580	360 041.449	1 151.438	1 200 717.576	360 041.447	1 151.443	1 200 717.576	360 041.447	1 151.443
	5003	0 526.676	59 994.048	22.861	0 526.677	59 994.046	22.866	0 526.676	59 994.046	22.865
	5004	0 416.323	59 697.272	48.785	0 416.323	59 697.270	48.782	0 416.323	59 697.270	48.782
	5005	0 404.622	59 628.282	53.725	0 404.621	59 628.281	53.729	0 404.621	59 628.281	53.729
	5006	0 722.287	59 376.690	60.937	0 722.285	59 376.691	60.939	0 722.286	59 376.690	60.939
	5007	1 034.329	59 371.645	58.930	1 034.328	59 371.646	58.934	1 034.328	59 371.645	58.935
^{11}t	5002	1 200 717.577	360 041.448	1 151.438	1 200 717.577	360 041.447	1 151.439	1 200 717.577	360 041.447	1 151.439
	5003	0 526.675	59 994.049	22.861	0 526.674	59 994.050	22.861	0 526.675	59 994.050	22.860
	5004	0 416.320	59 697.279	48.785	0 416.319	59 697.279	48.786	0 416.319	59 697.279	48.786
	5005	0 404.615	59 628.285	53.725	0 404.613	59 628.285	53.726	0 404.613	59 628.285	53.726
	5006	0 722.292	59 376.694	60.937	0 722.291	59 376.694	60.939	0 722.290	59 376.694	60.940
	5007	1 034.333	59 371.650	58.930	1 034.332	59 371.650	58.930	1 034.331	59 371.650	58.931

Subsequently, transformed coordinates in the national implementation UTCN03 from all three adjustments and three epochs of observations were used for the next presentation of positional and vertical changes of individual network points. 2 graphical visualisations (Fig. 2) of positional and vertical changes of points from epochs $^{08}t, ^{11}t$ to the epoch ^{04}t for all three methods of adjustment of observations were created.

The overall displacements of points corresponded to changes of coordinates presented in the deformation analysis, coordinates of which were determined by the LSM method and robust M-estimation according to Huber and Hampel. Difference of displacements is caused by dependence of cofactors on the size of weights of individual methods. The analysis of the results obtained from processing was performed by the method of finite elements in the form of strain analysis, to present the dynamics of the area underneath the water reservoir (Strain analysis can be applied only to the homogenous environment).

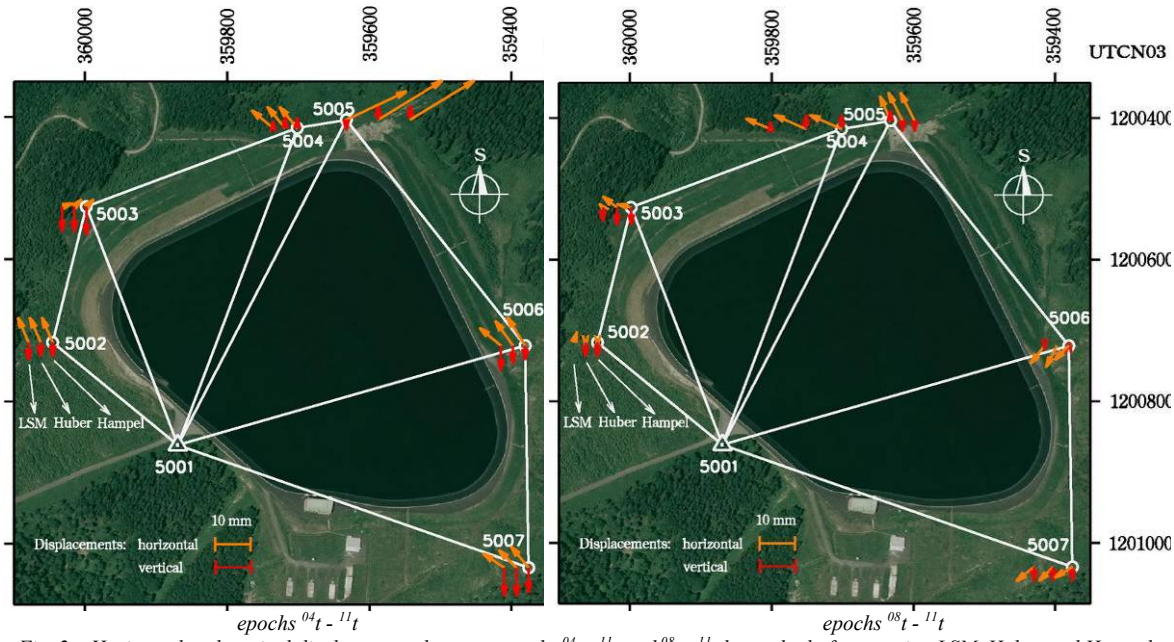

Fig. 2. Horizontal and vertical displacements between epochs ${}^{04}t$ - ${}^{11}t$ and ${}^{08}t$ - ${}^{11}t$ by method of processing LSM, Huber and Hampel

Deformation strain analysis

The strain analysis is used to describe deformations in the vicinity of point. The spatial deformation of object with its small surrounding can be expressed by coordinates [17]:

$$ {}^{\tau,\tau+1}\Delta\hat{C}_i = {}^{\tau+1}\hat{C}_i - {}^{\tau}\hat{C}_i = {}^{\tau,\tau+1}\varepsilon\,{}^{\tau+1}\hat{C}_i + {}^{\tau,\tau+1}T_i \tag{9}$$

where: τ=04,08,11; ${}^{\tau,\tau+1}T$ is the vector of translation parameters of the point expressing its spatial change over the period $\Delta t = {}^{\tau+1}t - {}^{\tau}t$ in all coordinate directions:

$$ {}^{\tau,\tau+1}T_i = \begin{pmatrix} {}^{\tau,\tau+1}T_X \\ {}^{\tau,\tau+1}T_Y \\ {}^{\tau,\tau+1}T_h \end{pmatrix}_i \tag{10}$$

If displacements are very small in comparison with the size of object, results in the deformation tensor ε_i represent the tensor of overall deformation in the following form [4], [17]:

$$ {}^{\tau,\tau+1}\varepsilon_i = {}^{\tau,\tau+1}\begin{pmatrix} \frac{\partial\Delta X}{\partial X} & \frac{\partial\Delta X}{\partial Y} & \frac{\partial\Delta X}{\partial h} \\ \frac{\partial\Delta Y}{\partial X} & \frac{\partial\Delta Y}{\partial Y} & \frac{\partial\Delta Y}{\partial h} \\ \frac{\partial\Delta h}{\partial X} & \frac{\partial\Delta h}{\partial Y} & \frac{\partial\Delta h}{\partial h} \end{pmatrix}_i = {}^{\tau,\tau+1}\begin{pmatrix} \varepsilon_{XX} & \varepsilon_{XY} & \varepsilon_{Xh} \\ \varepsilon_{YX} & \varepsilon_{YY} & \varepsilon_{Yh} \\ \varepsilon_{hX} & \varepsilon_{hY} & \varepsilon_{hh} \end{pmatrix}_i, \tag{11}$$

where $\Delta X, \Delta Y$ and Δh are 3 components of the displacement vector ${}^{\tau,\tau+1}\Delta\hat{C}_i$. Due to the asymmetry of deformation tensor ε_i, it is possible to decompose it into the symmetrical and asymmetrical part according to the following equation:

$$ \varepsilon_i = e_{ij} + \omega_{ij} = \frac{1}{2}.\left(\varepsilon_{ij} + \varepsilon_{ij}^T\right) + \frac{1}{2}.\left(\varepsilon_{ij} - \varepsilon_{ij}^T\right) \tag{12}$$

where the symmetrical part of deformation tensor ε_i is referred to as the strain tensor e_{ij} and asymmetrical part of deformation tensor ε_i represents the rotation ω_{ij}. Tensor diagonal elements e_{ii} are referred to as the tensile strain and characterize a dilatation in the appropriate direction. Off-diagonal elements are referred to as shear strains and characterize changes in angles between appropriate input lines.

Graphical interpretation of elements of the strain tensor e_{ij} (12) on the example of cube (Fig. 3) with edges of uniform lengths that is plotted by thin lines and its deformed shape by thick line with designation of relevant changes due to the deformation.

The rotational component ω_{ij} can be split into two parts: the component dependent on the position ω'_{ij} and independent on the position ω°_{ij}. The computational procedure of components of the strain tensor e_{ij} is a matter of simple transformation for any direction.

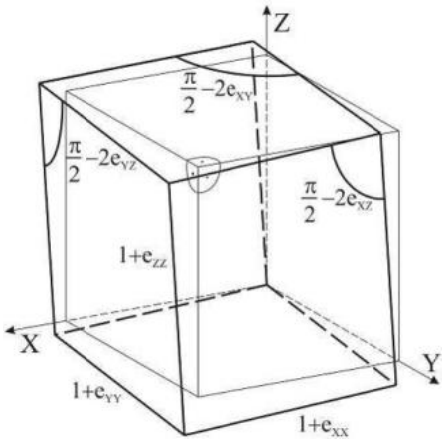

Fig. 3. Geometrical interpretation of strain elements

Strain analysis of the DN points in the XY plane

Deformation strain analysis can be used not only for analysis of 2D (or 3D) physical changes in the entire monitored area, but also for its individual parts, while results of these strain analyses are more trustworthy. The smaller parts of the area of triangular shape in the total number of 5 (Fig. 4) were created by suitable triples of points of the geodetic network around the crest of upper reservoir of the PSHPP Čierny Váh. The spatial displacement of the i-*th* point for the monitored period can be expressed by the following equation [4], [17]:

$$\underset{(2,1)}{\Delta XY_i} = \begin{pmatrix} \Delta X \\ \Delta Y \end{pmatrix}_i = \left(\begin{pmatrix} e_{xx} & e_{xy} \\ e_{yx} & e_{yy} \end{pmatrix} + \begin{pmatrix} 0 & \omega_{xy} \\ -\omega_{yx} & 0 \end{pmatrix} \right) \cdot \begin{pmatrix} X \\ Y \end{pmatrix}_i + \begin{pmatrix} T_x \\ T_y \end{pmatrix}, \qquad (12)$$

where $\begin{pmatrix} X \\ Y \end{pmatrix}_i$ are the point coordinates in the 2. epoch of analysis and the vector of deformation parameters:

$$\underset{(1,6)}{\theta^T} = \begin{pmatrix} e_{xx} & e_{xy} & e_{yy} & \omega_{xy} & T_x & T_y \end{pmatrix}^T \qquad (13)$$

includes all remaining unknown points from the equation (13).

Vector ΔXY_i represents a displacement of point and its surroundings in the direction of coordinate axes:

$$\Delta XY_i = F_i \cdot \theta, \qquad (14)$$

where F_i is the matrix of coefficients containing point coordinates of the second epoch:

$$\underset{(2,6)}{F_i} = \begin{pmatrix} X_i & Y_i & 0 & Y_i & 1 & 0 \\ 0 & X_i & Y_i & -X_i & 0 & 1 \end{pmatrix}. \qquad (15)$$

For individual areas of triangular shape, it is possible to express deformation parameters θ binding to three points. By mathematical expression of θ from the equation (15) and by addition of their weights Q, the following relation can be defined:

$$\theta = \left(F^T \cdot Q^{-1}_{\Delta XY} \cdot F \right)^{-1} \cdot F^T \cdot Q^{-1}_{\Delta XY} \cdot \Delta XY. \qquad (16)$$

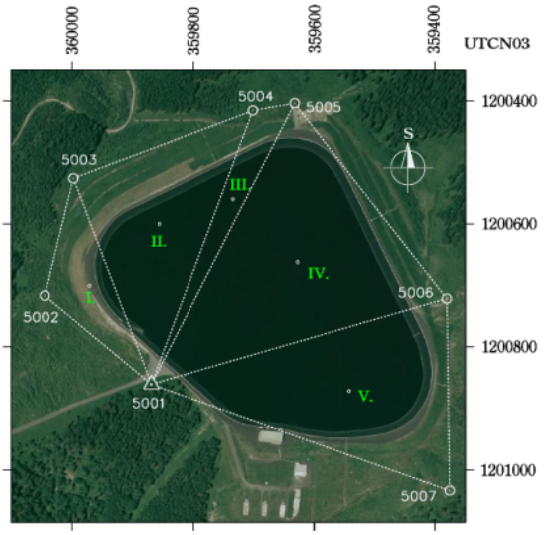

Legend: ° – *location of the centre of gravity of triangular shape area,*
I. – V. – *the number of triangular shaped area.*
Fig. 4. Parts of the area around the PSHPP Čierny Váh

Tab. 3. Deformation parameters of the strain analysis 04/11 and 08/11.

	area part Δ	e_{xx} [μstrain]		e_{xy} [μstrain]		e_{yy} [μstrain]		ω_{xy} [´´]		T_x [m]		T_y [m]	
		04/11	08/11	04/11	08/11	04/11	08/11	04/11	08/11	04/11	08/11	04/11	08/11
LSM	I.	-17,912	-5,190	-15,924	-14,413	35,573	-11,858	-7,946	-1,419	0,041	0,014	-0,040	0,013
	II.	7,136	4,873	4,235	-2,236	-29,451	-16,722	1,359	1,478	-0,012	-0,008	0,013	0,017
	III.	-5,533	-16,167	-52,136	10,291	358,588	64,785	19,916	10,402	-0,009	-0,002	0,050	0,025
	IV.	14,307	24,192	28,623	-9,934	-26,891	-7,408	-4,637	-1,488	-0,019	-0,023	-0,052	0,006
	V.	3,355	-3,355	4,538	-3,107	-12,222	-9,060	0,977	-1,272	-0,007	0,007	0,005	0,000
Huber	I.	-13,560	16,236	-16,315	0,795	32,003	-14,279	-7,129	3,755	0,035	-0,026	-0,033	0,026
	II.	9,746	8,961	3,576	-8,030	-22,582	-10,862	1,295	1,664	-0,015	-0,011	0,011	0,023
	III.	-14,816	-13,770	-35,656	4,771	358,184	81,084	22,821	11,456	-0,009	-0,005	0,047	0,032
	IV.	19,517	28,004	30,585	-13,408	-25,222	-4,272	-4,505	-1,419	-0,027	-0,026	-0,054	0,009
	V.	6,610	-6,577	6,135	-3,653	-10,185	-7,023	1,299	-1,391	-0,012	0,012	0,004	-0,001
Hampel	I.	-13,560	7,533	-16,315	-2,775	32,003	-14,279	-7,129	3,018	0,035	-0,013	-0,033	0,026
	II.	9,746	6,005	3,576	-4,110	-22,582	-10,862	1,295	2,472	-0,015	-0,010	0,011	0,023
	III.	-14,816	-13,770	-35,656	4,771	358,184	81,084	22,821	11,456	-0,009	-0,005	0,047	0,032
	IV.	18,271	25,514	31,786	-10,383	-25,222	-6,674	-4,257	-1,051	-0,026	-0,025	-0,054	0,009
	V.	6,643	-3,322	7,153	-2,089	-10,185	-9,060	1,509	-1,062	-0,013	0,007	0,004	0,000

The strain analysis for a pair of epoch - and - was performed in the Matlab 7.12.0 software for point coordinates determined by using the LSM method and robust M-estimations according to Huber and Hampel (Tab. 3).

Graphical interpretation of the strain analysis

In addition to numerical interpretations of the result of strain analysis, it is also possible to interpret them in a graphical way, and therefore it is possible to obtain clear information on deformations that occurred within the monitored locality [4], [13], [17]:

- *dilatation* Δ (a proportional planar deformation of the area) expresses the proportional change of the area between two examined epochs for the monitored area:

$$\Delta = e_{xx} + e_{yy}, \tag{17}$$

positive values represent expansion of the area part and negative values represent compression of the area part for the monitored period, which can be graphically displayed in the form of circles with a radius Δ in the unit of μstrain,

- *proportional shear deformation* γ :

$$\gamma = \sqrt{\left(e_{xx} - e_{yy}\right)^2 + \left(2.e_{xy}\right)^2}, \tag{18}$$

expresses proportional changes of real angles for the monitored period. It can be graphically interpreted by using isolines with numerical data in μstrain,

- *the size of horizontal displacements* Δh can be displayed by isolines from values:

$$\Delta h = \sqrt{T_x^2 + T_y^2}. \tag{19}$$

Character of deformations of the monitored area can be complemented by additional parameters [13]:

- the size of the major, maximum tensile deformation (dilatation, expansion) e_1 :

$$e_1 = 0{,}5.(\Delta + \gamma) \ \ [\mu strain], \tag{20}$$

- the size of the major, minimum tensile deformation (compression) e_2 :

$$e_2 = 0{,}5.(\Delta - \gamma) \ \ [\mu strain], \tag{21}$$

- the bearing of the axis of maximum tensile deformation e_1 σ_{e_1} :

$$\sigma_{e_1} = 0{,}5.arctg(2.e_{xy}/(e_{xx} - e_{yy})) \ \ [°], \tag{22}$$

- the bearing of the axis of shear deformation σ_γ :

$$\sigma_\gamma = \sigma_{e_1} \pm \pi/4 \ [°]. \tag{23}$$

Individual calculated parameters of the strain analysis for the parts of area of triangular shape determined from results adjusted by using the above estimation methods of unknown parameters are presented in Tab. 3.

Tab. 3. Values of proportional planar, proportional shear deformation and horizontal displacements.

$^{\tau}t$	Δ	LSM			Huber			Hampel		
		Δ	γ	Δh	Δ	γ	Δh	Δ	γ	Δh
		[μstrain]	[μstrain]	[mm]	[μstrain]	[μstrain]	[mm]	[μstrain]	[μstrain]	[mm]
04-11	I.	17,661	62,248	57,310	18,443	56,042	48,104	18,443	56,042	48,104
	II.	-22,314	37,554	18,321	-12,837	33,110	19,023	-12,837	33,110	19,023
	III.	353,055	378,757	50,388	343,368	379,755	47,677	343,368	379,755	47,677
	IV.	-12,583	70,528	55,209	-5,706	75,784	60,080	-6,951	77,027	59,804
	V.	-8,867	18,027	8,703	-3,574	20,800	13,000	-3,542	22,088	13,740
08-11	I.	-17,047	29,587	19,243	1,957	30,557	37,037	-6,747	22,507	29,248
	II.	-11,850	22,054	18,911	-1,902	25,512	25,615	-4,858	18,764	25,317
	III.	48,618	83,528	25,004	67,314	95,333	32,207	67,314	95,333	32,207
	IV.	16,784	37,328	23,637	23,732	41,963	27,950	18,840	38,306	26,551
	V.	-12,415	8,436	7,377	-13,601	7,320	11,701	-12,382	7,098	6,606

Fig. 5. circles displayed in orange represent compression of the triangular shaped part of the area (negative values of *dilatation* **Δ** from Tab. 3) and red circles expansion of the area (positive values of *dilatation* **Δ** from Tab. 3). Blue chain-dotted circles represent the size of proportional shear deformation for the period ^{04}t - ^{11}t and ^{08}t - ^{11}t related to the centre of gravity of that area (Tab. 3 - **γ**). The radius size of circles is dependent on the size of presented results in units of μstain.

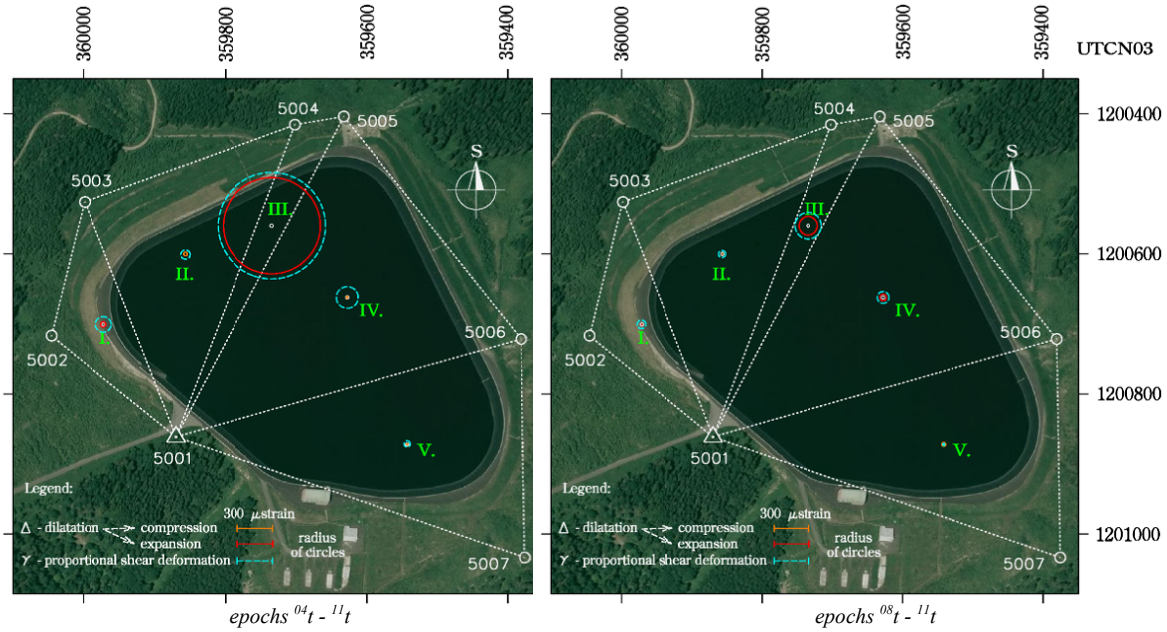

Fig. 5. Proportional planar and shear deformations displayed by circle by method of processing LSM, Huber and Hampel

Tab. 5 present the graphical representation of translations *Δh* by isolines with the basic interval of 10 mm related to the centre of gravity of that area (Tab. 3).

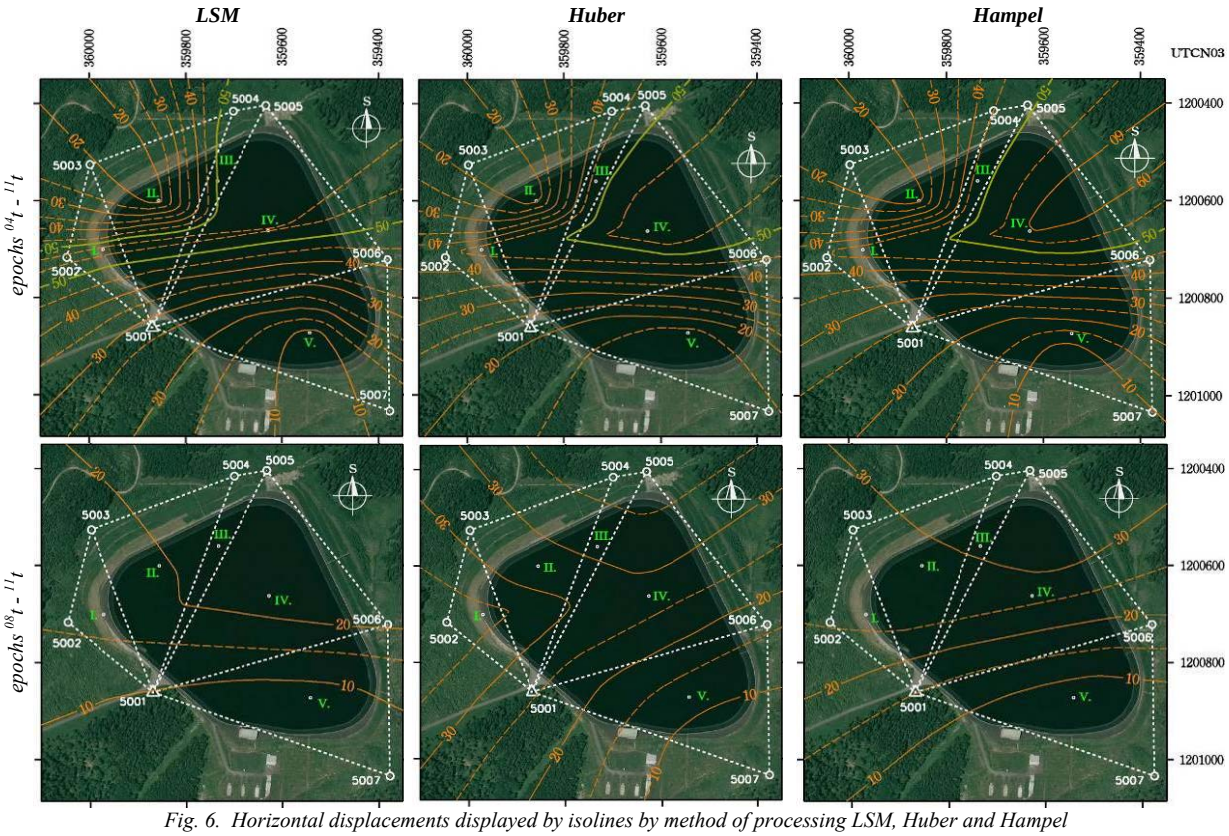

Fig. 6. Horizontal displacements displayed by isolines by method of processing LSM, Huber and Hampel

Conclusion

The present article provides an overall processing of the geodetic network and the deformation analysis of the area around and underneath the upper reservoir of the pumped storage hydro power plant (PSHPP) Čierny Váh in the 2004 – 2011. The analysis was realized based on the stage adjustment of GNSS vectors, by applying three selected methods of processing and adjustment of geodetic network with the estimation of unknown parameters. The LSM method, robust M-estimation according to Huber and robust M-estimation according to Humpel represented the selected methods of estimations. In the present study, the estimations of parameters of the 1st and 2nd order of network structures and their statistical assessment in the area of deformation monitoring were solved. For this purpose, a local geodetic network of reference points was surveyed by using GNSS technology in the locality of the pumped storage hydro power plant (PSHPP) Čierny Váh. The measurements were realized in three epochs (April 2004, July 2008 and October 2011) in a sufficient time interval.

In the article was the examination of incurred differences of adjusted coordinates of points in the deformation network resulting from the use of different methods for processing of measurements. However, displacement of the point 5005 was demonstrated by all three methods. Other differences were identified as the result of the effect of systematic and measurement errors. A graphical testing using absolute and relative confidence ellipsoids that confirmed the results obtained by processing was also realized. The strain analysis of the geodetic network was also performed in the process of deformation analysis, for the identification and transparent description of spatial changes in the monitored area underneath and around the water reservoir, for the selected period. The whole processing was performed in the Matlab 7.12.0 that was also used as the visualisation instrument for the presentation of estimations of results obtained from the geodetic network of the area.

References

[1] Bitterer, L.: Adjustment calculus (Vyrovnávací počet). *ŽU Žilina, 2006, 280 p., ISBN 80-8070-517-8.*

[2] Böhm, J., Radouch, V., Hampacher, M.: Error theory and adjustment calculus (Teorie chyb a vyrovnavací počet). *2nd edition, Praha: Geodetic and cartographic enterprise, 1990, 416 p., ISBN 80-7011-056-2.*

[3] Böhm, J., Radouch, V.: Adjustment calculus (Vyrovnávací počet). *Praha, Kartografie, 1978, 510 p., ISBN 29-909-78.*

[4] Caspary, W. F.: Concepts of network and deformation analysis. *1st edition, Kensingthon: School of surveying. The University of New South Wales, 1987, 187 p., ISBN 0-85839-044-2.*

[5] Gaňová, L., Zeleňáková, M., Purcz, P., Kuzevičová, Ž., Hlavatá, H.: A rainfall distribution and their influence on flood generation in the eastern Slovakia. *Acta Universitatis Agriculturae et Silviculturae Mendelianae Brunensis. 61, 2013, 6, 1645-1652, ISSN 1211-8516.* Available at: http://acta.mendelu.cz/pdf/actaun201361061645.pdf

[6] Gašincová S., Gašinec J., Staňková H., Černota P.: Comparison of LSM and alternative estimation methods of the processing results of geodetic measurements. *SDMG 2011: Proceedings of the 18th conference: Praha, 5.-7. 9. 2011. Ostrava, VŠB-TU, 2011, 40-50, ISBN 978-80-248-2489-5.*

[7] Gašinec J., Gašincová S., Černota P., Staňková H.: Uses of Terrestrial Laser Sanning in Mnitoring of Ground Ice within Dobšinská Ice Cave. *Journal of the Polish Mineral Engineering Society, 30, 2, 2012, 31-41, ISSN 1640-4920.* Available at: http://www.potopk.republika.pl/Full_text/im_30_a04_gasinec.pdf

[8] Gašinec, J. Gašincová, S., Gergeľová, M.: Creation of Spatial Model of Dobšinská Ice Cave and its Connection into the National Coordinate Reference System UTCN03. *Geodetic and cartographic horizon. 58, 2012, 9, 218-223, ISSN 0016-7096.* Available at: www.archivnimapy.cuzk.cz/zemvest/cisla/Rok201209.pdf

[9] Gergeľová, M., Kuzevičová, Ž., Kuzevič, Š.: A GIS based assessment of hydropower potential in Hornád basin. *Acta Montanistica Slovaca. 18, 2013, 2, 91-100, ISSN 1335-1788.* Available at: http://actamont.tuke.sk/pdf/2013/n2/4gergelova.pdf

[10] Gergeľová, M., Kuzevičová, Ž., Kuzevič, Š., Sabolová, J.: Hydrodynamic modeling and GIS tools applied in urban areas. *Acta Montanistica Slovaca. 18, 2013, 4, 226-233, ISSN 1335-1788.* Available at: http://actamont.tuke.sk/pdf/2013/n4/3gergelova.pdf

[11] Jäger, R., Müller, T. Saler, H., Schwäble, R.: Klassische und Robuste Ausgleichungsverfahren. *Wichmann, Heidelberg, 2005, 340 p., ISBN 3-87907-370-8.*

[12] Klobušiak, M., Leitmannová K., Ferianc, D.: Implementation of mandatory transformations national reference coordinate and elevation systems to ETRS89. [online, cited 20.3.2012]. Available at: www.gku.sk/docs/referaty/2005/Klobusiak.pdf.

[13] Kolcun, Š., Sütti, J.: Deformation analysis of the area around Jaslovské Bohunice. *Acta Montanistica Slovaca. 5, 2000, 1, 71-76, ISSN 1335-1788.* Available at: http://actamont.tuke.sk/pdf/2000/n1/14kolcunsutti.pdf

[14] Labant, S., Weiss, G., Kukučka, P.: Robust adjustment of a geodetic network measured by satellite technology in the Dargovských Hrdinov suburb. *Acta Montanistica Slovaca. 16, 2011, 3, 229-237, ISSN 1335-1788.* Available at: http://actamont.tuke.sk/pdf/2011/n3/7labant.pdf

[15] Mixtaj, L., Weiss, E., Weiss, R., Kukučka, P.: Impact of acquisition on financial indicators of mining. *SGEM 2013. 13th International Multidisciplinary Scientific Geoconference Science and Technologies in Geology, Exploration and Mining. Conference proceedings, 1, 16-22, June, 2013, Albena, Bulgaria, Albena, STEF92 Technology Ltd., 2013, 501-506, ISBN 978-954-91818-7-6*

[16] Naščáková, J., Weiss, E., Červenka, P., Mixtaj, L., Weiss, R.: A support of the renewable source energy utilization and conditions for the biogass station investment. *Acta Montanistica Slovaca. 14, 2009, 4, 323-329, ISSN 1335-1788.* Available at: http://actamont.tuke.sk/pdf/2009/n4/7nascakova.pdf

[17] Sabová, J., Jakub, V.: Geodetic deformation monitoring. *1st edition. Košice: Editor centre and editorial office AMS, F BERG, Technical University of Košice, 2007, 128 p., ISBN 978-80-8073-788-7.*

[18] Sabová, J., Pukanská, K.: Expansion of local geodetic point field and its quality. *GeoScience Engineering. 58, 2012, 3, 47-51, ISSN 1802-5420.* Available at: http://gse.vsb.cz/2012/LVIII-2012-3-47-51.pdf

[19] Sokol Š., Bajtala M., Ježko J., Černota P.: Testing the Accuracy of Determining 3D Cartesian Coordinates Using the Measuring Station S8 Trimble DR Plus ROBOTIC. *Journal of the Polish Mineral Engineering Society, 33, 1, 2014, 85–90, ISSN 1640-4920.* Available at: http://www.potopk.republika.pl/Full_text/IM%201-2014-a11.pdf

[20] Sütti, J., Weiss, G.: 3D geodetic monitoring slope deformations. *Acta Montanistica Slovaca. 1, 1996, 2, 109-116, ISSN 1335-1788.* Available at: http://actamont.tuke.sk/pdf/1996/n2/3sutti.pdf

[21] Vávrová, V., Weiss, E., Červenka, P., Ferencz, V., Naščáková, J.: Possibilities and problems of using pupillary reflex for subconscious detection of consumer preferences. *Metalurgija. 53, 2014, 1, 85-88, ISSN 0543-5846.* Available at: http://hrcak.srce.hr/file/153477

[22] Weiss, G., Sütti J.: Geodetic local network I (Geodetické lokálne siete). *Štrofek, 1997, 88 p., ISBN 80-967636-2-8.*

[23] Act No. 364/2004 Coll., on waters, amending Act No. 372/1990 Coll. of the Slovak National Council on offences, as amended by later regulations (Water Act).

[24] Decree no. 75/2011 Office of Geodesy, Cartography and Cadastre of the Slovak Republic of 15 March 2011, amending and supplementing Decree of the Office of Geodesy, Cartography and Cadastre of the Slovak Republic no. 300/2009 Coll., implementing no. 215/1995 Coll., of the National Council of the Slovak Republic about geodesy and cartography, as amended by later regulations.